analytical chemistry

pubs.acs.org/ac Article

Size and Shape Effects on Nanoparticle-Catalyzed Reactions Enabled by High-Throughput Variable-Temperature Desorption Electrospray Ionization Mass Spectrometry

Madison E. Edwards,[‡] Nabojit Kar,[‡] Dallas P. Freitas,[‡] Lingjie Zhang, Oluwasegun J. Wahab, Lane A. Baker,* Sara E. Skrabalak,* and Xin Yan*

Cite This: *Anal. Chem.* 2025, 97, 19544−19551 Read Online

ABSTRACT: Nanoparticles exhibit unique catalytic properties that are highly dependent on their size and shape, influencing reaction rates, selectivity, and efficiency. Identifying the structural effects that achieve a high catalytic performance is critical to a wide range of applications, from energy conversion to environmental remediation. High-throughput screening (HTS) methods, particularly desorption electrospray ionization mass spectrometry (DESI-MS), offer a powerful approach for rapidly assessing the catalytic performance of nanoparticles with varying sizes and shapes. DESI-MS enables the direct analysis of reaction products without sample preparation, making it ideal for screening homogeneous catalytic reactions. However, applying this technique to heterogeneous catalysts remains challenging, and the lack of temperature control limits its ability to reflect realistic reaction conditions. In this article, we present the development of high-throughput variable-temperature DESI-MS (HT-vT-DESI-MS), a novel approach that combines DESI-MS with thin-film reaction acceleration and precise temperature control. This advancement allows the study of size and shape effects on nanoparticle-catalyzed reactions under varied conditions, offering a rapid understanding of structural parameters influencing catalytic performance. Our results show that varying the size of cubic Pd nanoparticles from 10 to 20 nm significantly impacts catalytic activity in Suzuki cross-coupling and indole arylation reactions, with distinct changes in both the effective surface area and Pd concentration. For both reactions, the reactivity trend normalized to the effective surface area was 10 nm cubic > 15 nm cubic > 20 nm cubic and normalized to the NP number was 20 nm cubic > 15 nm cubic > 10 nm cubic. Additionally, altering the nanoparticle shape from cubic to octahedral results in a marked decrease in product conversion, highlighting the critical role that nanoparticle morphology plays in determining catalytic efficiency. This research provides a HTS method for nanoparticle catalysts that can accelerate identification of design principles for their use in various catalytic applications.

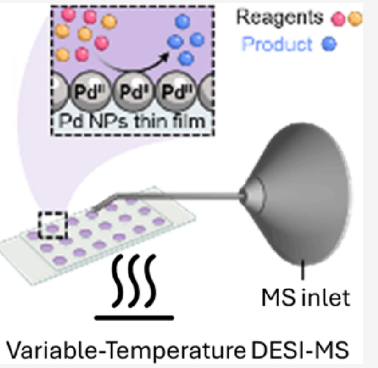

Nanoparticle (NP) catalysis has long been recognized as a powerful approach for enhancing reaction efficiency, with catalytic NPs offering high activity as heterogeneous catalysts due to the large surface area-to-volume ratio and the surface-confined nature of active catalytic sites. The unique structural and electronic properties of metal NPs enable exceptional activity and selectivity, making them indispensable in a wide range of chemical transformations. NPs have demonstrated broad utility in promoting carbon−carbon and carbon−heteroatom bond formation, especially in cross-coupling reactions such as Mizoroki−Heck,[1−4] Suzuki,[1,3−5] Pauson−Khand allylation of nucleophiles,[6,7] Stille-type,[3,4] and Sonogashira.[4] These systems benefit from the high activity and potential recyclability offered by heterogeneous NP catalysts. Over the past few decades, extensive research has focused on how NP structural features, including size, shape, and crystallographic orientation, influence catalytic behavior, particularly through reactions localized at undercoordinated edge, corner, and high-index facet sites.[8] These reactive sites are often key determinants of catalytic performance, particularly in bond-forming reactions that are central to organic synthesis.

Colloidal synthesis has played a pivotal role in advancing this field by enabling nanocrystals with well-defined morphologies and surface atom distributions to be achieved.[9] This control has sparked considerable interest in understanding structure−activity relationships in noble metal NPs, which are widely used in applications ranging from fine chemical synthesis to energy conversion. In particular, shape-controlled NPs have proven essential in elucidating the role of specific surface

Received: April 29, 2025
Revised: August 24, 2025
Accepted: August 25, 2025
Published: September 2, 2025

https://doi.org/10.1021/acs.analchem.5c02537
Anal. Chem. 2025, 97, 19544−19551

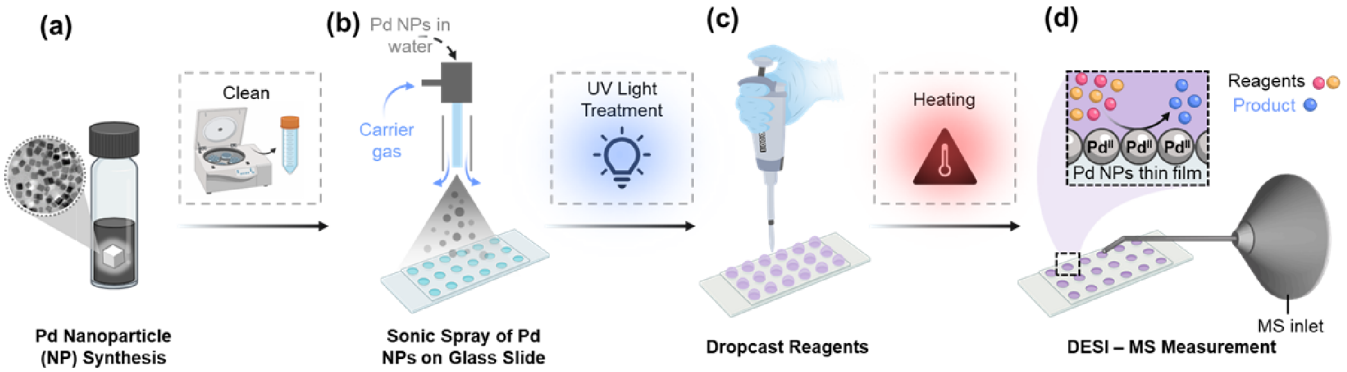

Figure 1. Workflow for screening of NP-catalyzed thin-film reactions, including (a) colloidal synthesis of NPs and a washing step to remove capping agents from the NP synthetic protocol and (b) sonic spray of the NPs onto the surface containing small wells for reaction screening. The NPs are adhered to the surface overnight under UV light, which serves as a second cleaning step to remove capping agents. (c) Dropcasting the reagents into the NP-containing wells allows for a reaction to be initiated, and the reactions are completed through heating the glass surface in a closed system. (d) The reactions are screened via MS analysis using a homemade DESI stage.

planes in catalytic processes.[10] For example, a study has demonstrated that palladium (Pd) NPs featuring surface facets exhibit superior catalytic reactivity in Suzuki−Miyaura coupling reactions compared to those with {111} facets.[11] These results are due to the interaction of O_2 with the Pd on the NP surface leading to differing leaching susceptibility of the {100}- and {111}-faceted NPs.[11]

To accelerate discovery in this space, high-throughput screening (HTS) techniques are increasingly being adopted for the rapid evaluation of catalytic reactions. For instance, microdroplets have recently emerged as a unique chemical reactor capable of accelerating reactions by an order of magnitude or more. These reactions occur in various formats, including spray-based (electrospray and sonic spray), microdroplet collisions, splashing onto surfaces, levitated droplets, and thin films. Reaction acceleration in microdroplets is attributed to their high surface-area-to-volume ratio, increased local reagent concentrations due to solvent evaporation, and partially solvated states that reduce activation energy compared to bulk-phase reactions. Desorption electrospray ionization mass spectrometry (DESI-MS) has shown particular promise for such applications due to its ability to analyze solution-phase reaction products under ambient conditions without sample workup or chromatographic separation. This attribute has made DESI-MS an attractive option for screening homogeneous catalytic reactions. However, its application in heterogeneous catalysis, especially NP-catalyzed systems, has been limited by several challenges, including inefficient product desorption from solid supports and a lack of temperature control, which restrict its utility for reflecting realistic reaction conditions. In fact, very few high-throughput MS methods currently exist for screening NP-catalyzed reactions. One method, developed by Banerjee et al., utilizes an NP-doped filter paper to screen three model reactions with Pd and silver (Ag) NPs via paper spray ionization MS.[12] Reactive paper spray ionization MS provides rapid screening of reactions employing a thin liquid film that acts as a microreactor.[13] An example reaction with Pd NPs was a Suzuki coupling reaction that involved phenylboronic acid with either bromophenylacetic acid or 4-bromophenol, which has conversion ratios of 7 and 3%, respectively.[12] However, this method cannot accommodate a reaction temperature other than that at room temperature.

In this work, we address these limitations through the development of high-throughput variable-temperature DESI-MS (HT-vT-DESI-MS), a novel platform that integrates DESI-MS with thin-film reaction acceleration and precise temperature modulation. This innovative approach enables rapid and reproducible assessment of NP-catalyzed reactions under tunable thermal conditions, while maintaining compatibility with solid-supported and surface-confined systems. By leveraging the thin-film reaction format, an implementation of microdroplet acceleration in confined volumes,[14] reactions are restricted to nanoscale layers, which enhances diffusion and accelerates reaction kinetics, allowing for efficient screening of NP catalysts. Moreover, this approach is compatible with strategies to remove capping agents used in colloidal NP synthesis, providing both insights into how capping agents can interact with catalysis and also insights into the intrinsic facet-dependent activity of NPs.

In this method, NPs are first synthesized using a colloidal approach, followed by an initial cleaning step to remove excess capping agents from the synthetic media. The cleaned NPs are then deposited onto glass slides using sonic spray, a technique that can be adapted for alternative substrates, such as optically transparent electrodes,[15] for NP imaging. To ensure complete removal of the capping agents, we then exposed the deposited NPs to UV illumination overnight. The glass slides contain small wells (circular with a diameter of 4 mm), into which reaction reagents are dropcast directly onto the dried NPs for thin-film reactions on the surface at a desired temperature, followed by high-throughput DESI-MS analysis (Figure 1).

Our results show that the smallest Pd NPs studied (10 nm cubes) exhibit the highest catalytic activity when normalized to their effective surface area. However, when normalized to the Pd concentration, the largest Pd NPs studied (20 nm cubes) demonstrate higher conversion efficiency. By examining the influence of NP shape and size alongside the instrumentation setup, we provide an HTS method for NP catalysts for both Suzuki coupling and indole arylation reactions. These results open broadly a pathway for accelerated NP design for catalytic processes broadly.

EXPERIMENTAL SECTION

Materials and Reagents. For NP synthesis, sodium tetrachloropalladate (Na_2PdCl_4), L-ascorbic acid (AA), poly(vinylpyrrolidone) (PVP, MW ≈ 55,000), and potassium

https://doi.org/10.1021/acs.analchem.5c02537
Anal. Chem. 2025, 97, 19544−19551

bromide (KBr) were all purchased from Sigma-Aldrich. All chemicals were used as received without further purification.

For high-throughput NP-catalyzed reaction screening, all of the reagents were of analytical or chromatographic grade and were used without further purification. Suzuki coupling reagents 2-bromo-5-methylpyridine and phenylboronic acid were purchased from Acros Organics (Morris Plains, NJ). Methanol, ethyl acetate, and water were purchased from Sigma-Aldrich (St. Louis, MO). Sodium acetate was purchased from Combi-Blocks (San Diego, CA). For the tryptophan arylation reaction, H-Trp-OH (tryptophan) was purchased from aablocks (San Diego, CA) and 4-methoxybenzenediazonium tetrafluoroborate was purchased from Combi-Blocks (San Diego, CA). Acetic acid (LC/MS) was purchased from Thermo Fisher Scientific (Waltham, MA). PTFE-coated glass slides, purchased from SPI Supplies (West Chester, PA), were used as the DESI substrate.

For the reaction screening in Suzuki coupling catalyzed by Pd NPs, all reagents were purchased and not synthesized. 2-Bromo-5-methylpyridine was purchased from Arcos Organics (Morris Plains, NJ). Sodium acetate was purchased from Combi-Blocks (San Diego, CA). HPLC-grade solvents methanol, ethyl acetate, and water were purchased from Sigma-Aldrich (St. Louis, MO), and acetic acid was purchased from Thermo Fisher Scientific (Waltham, MA). PTFE 18-well glass slides were purchased from SPI Supplies (West Chester, PA).

Synthesis of Palladium (Pd) Nanoparticles (NP). Pd nanocubes of three different edge lengths (10, 15, and 20 nm; Figure S1) were synthesized with slight alterations to a published procedure.[16,17] A standard procedure involved filling an 8-dram (20 mL) vial with 8.0 mL of deionized water, 105 mg of PVP, and varying amounts of KBr and AA. The vial was then heated in an oil bath at 80 °C while stirring the solution at 400 rpm for 15 min. During this heating process, 3 mL of an aqueous Na_2PdCl_4 solution (19 mg/mL) was prepared in a separate vial with intermittent 30 s sonication. After 15 min of heating, the 3 mL Na_2PdCl_4 solution was rapidly added to the 20 mL vial (containing 8.0 mL of water, PVP, KBr, and AA) using a pipet. The addition of KBr and AA in the specified quantities produced nanocubes with edge lengths of 10 nm (303 mg of KBr and 60 mg of AA), 15 nm (900 mg of KBr and 20 mg of AA), and 20 nm (900 mg of KBr and 60 mg of AA). Each reaction was subsequently allowed to proceed at 80 °C for 3 h while stirring at 400 rpm.

After the reaction, 5 mL of deionized water was added to the reaction mixture without cooling, and the reaction mixture was then centrifuged. For nanocubes with edge lengths of 10 and 15 nm, the reaction mixture was divided into several 2 mL microcentrifuge tubes and centrifuged at 21,130*g* for 15 min. For nanocubes with edge lengths of 20 nm, the reaction mixture was added to a 50 mL centrifuge tube and centrifuged at 11,404*g* for 20 min. After each round of centrifugation, the dark black pellet was retained and the supernatant was discarded. These washing steps were repeated four times with deionized water. After washing, the Pd nanocubes were stored in deionized water (Figure S2).

Spraying of NPs onto the Substrate. To accomplish spraying of NPs prior to reaction screening, it was necessary to create a platform capable of a consistent, repeatable spray coating (Figures S3−S5). To accomplish this, we adapted a 3D printer into a pneumatic spraying system, inspired by Tucker et al.[18] A Monoprice (Rancho Cucamonga, CA) MP10 3D printer was used as the starting platform for the sprayer system due to its large bed size (300 mm × 300 mm) and bed plate heating. Adaptation was achieved by the replacement of the filament extruder assembly with a custom ESI spray source fitted using a custom-modeled 3D print. An ESI emitter was created by connecting a 150 μm OD, 50 μm ID fused silica inner capillary (for solvent) (BGB; Alexandria, VA) through a 0.020″ ID high-pressure PEEK tee body (Cole-Parmer; Northbrook, IL) connected using NanoTight sleeves (IDEX; Northbrook, IL). On the opposite end facing the build plate, stainless-steel tubing was used for sheath gas output at a height higher than the theoretical position of the filament nozzle to ensure no collision with the printer bed. Nitrogen gas was connected to the PEEK body using an external gas tank and a multistage regulator (Fisherbrand; San Diego, CA). The inner capillary was connected to a PEEK body unit (IDEX; Northbrook, IL). The opposite end of the union was connected to a Hamilton 1000 μL syringe (Reno, NV) connected to a syringe pump (Harvard Apparatus; Holliston, MA) For additional pneumatic sprayer parameters, see the Supporting Information.

Pd NPs were uniformly deposited onto the surface using a pneumatic spraying system adapted from a 3D printer described above, which automated the process and minimized human error. During optimization, we varied the number of spray passes (i.e., layers) and determined that 10 layers provided the optimal balance between the film thickness and catalytic performance, as measured by the conversion ratio.

Desorption Electrospray Ionization (DESI) Mass Spectrometry. A custom DESI source was fabricated using a PEEK high-pressure tee body (ID 0.020″ OD 1/16″; 10−32 coned) (Cole-Parmer; Vernon Hills, IL) with NanoTight sleeves (IDEX; Northbrook, IL), a PEEK union (0.010″ through; IDEX; Northbrook, IL), and a fused silica capillary (ID 200 μm, OD 360 μm) for the spray solvent and a fused silica capillary (ID 50 μm, OD 150 μm) for sheath gas (BGB; Alexandria, VA). The spray solvent, methanol, was loaded in a Hamilton 1000 μL syringe (Reno, NV) and pumped through the fused silica capillary via a syringe pump (Fusion 6000X, Chemyx, Inc.; Stafford, TX) at 8 μL/min. Nitrogen gas was used as the sheath gas at a pressure of 80 psi. High voltage (supplied from the mass spectrometer) was applied to the syringe needle at an application of 0−4.5 kV with minimal differences observed between high and low voltages. The emitter was placed approximately 2 mm (optimized each run for droplet generation) from the surface of the substrate at a 35° angle and 2 mm from the MS inlet. The MS inlet was constructed using smooth-bore seamless 316 stainless-steel tubing (OD 1/16″ and a wall thickness of 0.02″) cut to a length of 180 mm for LTQ and 225 mm for Orbitrap MS analysis; the MS inlet was also bent to a 20° angle to aid in surface sampling; the tubing was attached to the MS with a homemade adapter that was screwed into the MS interface.

The DESI stage was built to be a universally adaptive stage that can easily be modified for additional features, similar to the stage fabricated in recent literature (Figure S6).[19] An aluminum breadboard base (12 in. × 12 in. × 3/8 in.) was used to hold and connect each piece (Thorlabs; Newton, NJ). The main structure consisted of two *XY* translational stages (50 mm) that are stacked together like a cross; this creates the moving stage (Thorlabs; Newton, NJ). A 25 mm *XYZ* translational stage (Thorlabs; Newton, NJ) on the side was equipped with an optic rotation mount (Newport; Irvine, CA)

https://doi.org/10.1021/acs.analchem.5c02537
Anal. Chem. 2025, 97, 19544−19551

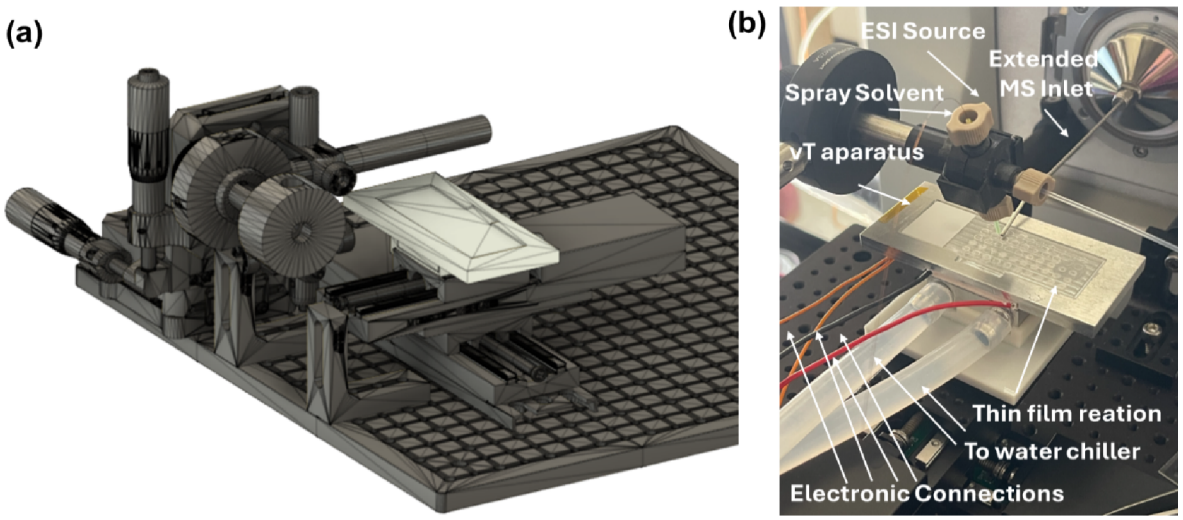

Figure 2. (a) 3D model of the vT-DESI stage, combining the homemade DESI stage (black) and the variable-temperature apparatus (gray). (b) Experimental view.

that can control the height, position, and orientation of the DESI source.

MS analysis was conducted on an LTQ-XL (Suzuki reaction) and Q Exactive Orbitrap (tryptophan arylation) mass spectrometer. The capillary temperature was set to 275 °C.

Variable-Temperature DESI (vT-DESI) Platform. A glass slide (Fisher Scientific, CA) was placed onto a custom-built machined aluminum heat exchanger (Figure S7). The heat exchanger was placed on top of a single-stage Peltier chip (TEC1-12706) using heat conductive CryoFuze thermal paste (Cooler Master, Taiwan). The Peltier chip was connected to a TC-720 thermoelectric temperature controller (TE Technology, United States) where the temperature was monitored using an MP-3193 15 kΩ thermistor in contact with the heat exchanger. Temperature was controlled by using the supplied software. The TC-720 was powered using a MEAN WELL LRS-100-24 (MEAN WELL. Taiwan) at 24 V DC. Power from the MEAN WELL was applied to a DC buck converter (Drok, China) to step down from 24 V DC to 6 V, 6 A. The converter was connected to the TC-720 to modulate and control the temperature of the Peltier chip. On the backside of the Peltier chip, a water-cooled heat exchanger was attached by using a 2 mm thermal pad (Iceberg Thermal, AZ) for easy attachment and removal. The water-cooled heat exchanger was connected to a BIQU water cooling kit (BIQU, China) to add/remove heat without compromising the thickness. This cooler was powered by using a 12 V DC power supply. A diagram of this is shown in Figure S8.

Prior to utilization of the vT-DESI stage, the temperature stability was monitored using this setup (Figure S9). Temperature was monitored during two critical time periods: when the glass slide was placed on the vT-DESI stage and when the initial DESI spray was started and moments after. It takes approximately 70 s to restabilize to temperatures above a set 75 °C with stability ±1 °C of the set target (Figure S10a). After the DESI spray is initiated for analysis (Figure S10b), it takes approximately 84 s to return to temperature with stabilization soon after. With this information, we validate consistent temperature output when coupled with DESI-MS analysis.

RESULTS AND DISCUSSION

Development of a Variable-Temperature DESI Platform with Integrated Thin-Film Acceleration for High-Throughput NP-Catalyzed Reaction Screening. A variable-temperature DESI (vT-DESI) system was developed for the high-throughput MS screening of temperature-dependent NP-catalyzed reactions (Figure 2 and Figure S9). The stage consists of a glass slide placed on a custom aluminum heat exchanger, mounted on a Peltier chip with CryoFuze thermal paste for efficient heat transfer. A 15 kΩ thermistor and thermoelectric controller regulate temperature, powered by a 24 V DC supply stepped down to 6 V. A water-cooled heat exchanger, attached with a 2 mm thermal pad, dissipates heat while maintaining compact dimensions. The DESI sprayer and stage were aligned to accommodate variable-temperature analysis. The system achieves stable surface temperatures from 10−90 °C with ±1 °C precision. Temperature restabilizes within 70−84 s after slide placement and DESI spray (Figure S10), enabling reliable high-throughput, temperature-sensitive MS workflows.

To enhance the efficiency of NP-catalyzed reaction screening, a thin-film reaction acceleration feature was incorporated into the vT-DESI system. The Suzuki cross-coupling between phenylboronic acid and 2-bromo-5-methylpyridine, catalyzed by 20 nm cubic Pd NPs, was selected as a model reaction (Figure 3a and Figure S1f). This widely used C−C bond-forming reaction typically relies on phosphine-based Pd catalysts and requires prolonged heating (10−12 h at 100 °C) in bulk solution, which is incompatible with rapid screening methods such as DESI-MS. To overcome this limitation, a thin-film format was developed using dropcast microdroplets of the reaction mixture into wells on a PTFE-coated glass slide, enabling high-throughput analysis with enhanced reaction rates.

The reaction mixture (25 mM 2-bromo-5-methylpyridine, 50 mM phenylboronic acid, and 50 mM sodium acetate in methanol/water (v/v = 1/1)) was dropcast (1 μL) onto the substrate after 1 ppm Pd NPs were sonically sprayed onto the substrate. The reaction mixture was then allowed to react with the Pd NPs over an hour. Reactions were monitored by DESI-MS at 10 min intervals using an incubation chamber during

https://doi.org/10.1021/acs.analchem.5c02537
Anal. Chem. 2025, 97, 19544−19551

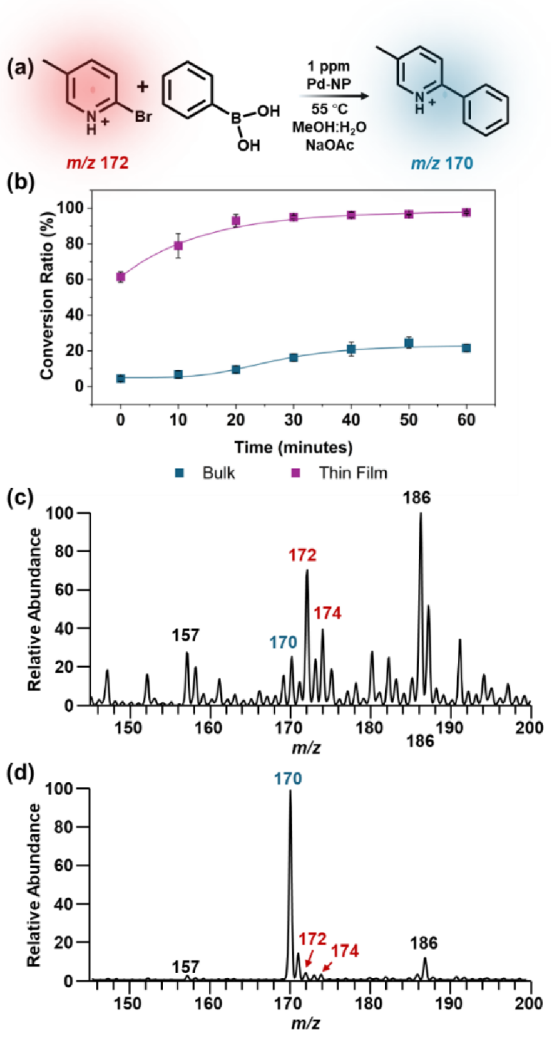

Figure 3. (a) Scheme of the Suzuki cross-coupling reaction. (b) Conversion ratio (%) of bulk solution (blue) and thin-film (purple) reactions using MS intensities. (c) Mass spectrum of heated bulk solution at 30 min with the reagent 2-bromo-5-methylpyridine in red (m/z 172). (d) Mass spectrum of heated thin-film reaction at 30 min with the product observed at m/z 170 in blue.

heating (see the Supporting Information for details). An incubation chamber was used to allow for reactions to be completed over prolonged times with the reaction time controlled by the time the reaction was heated. When the vT-DESI stage was used to heat the reaction in an open system, the reaction came to completion in minimal time (less than a minute) as shown by the linearity of the vT-DESI heating kinetics in Figure S11. The reaction performed in bulk solution heated to 55 °C with identical reagent conditions (Figure S12a) was compared to the thin-film reaction at the same temperature (Figure S12b and Figure 3b).

The results, summarized in Figure 3b–d, show dramatic differences in conversion efficiency between confined volume microdroplet reactions (<1 μL) and their bulk-solution, larger volume counterparts (>1 mL). After 60 min at 55 °C, the thin-film reaction reached a conversion ratio of 98%, while the reaction in bulk solution reaction showed only 22% conversion. Notably, when these reactions were conducted at room temperature, the thin-film reaction still reached 91% conversion compared to just 4% in bulk solution (Figure S13 and Tables S1 and S2). Conversion was calculated using DESI-MS signal intensities as $I_p/(I_r + I_p)$, where I_p corresponds to the product (m/z 170) and I_r to the unreacted starting material (m/z 172) (eq S1 and Tables S1 and S2). These data confirm that the combination of thin-film format with heating on the vT-DESI platform significantly accelerates NP-catalyzed transformations and enables rapid assessment of reaction progress (Figure 3). Error bars shown in Figure 3b reflect the small variations in conversion ratios across 6–9 repeated thin-film reactions. The system is especially suited for exploring temperature-sensitive pathways, where rapid feedback and low reagent volumes are critical. This integrated approach demonstrates a robust, high-throughput platform for NP-catalyzed reaction screening, leveraging the synergistic effects of the thin-film reaction acceleration and localized temperature control using vT-DESI-MS.

Additionally, the capping agent (PVP) used during the NP synthesis was removed (see the Supporting Information) from the NPs prior to catalysis yielding a 30% higher conversion ratio during catalysis (Figure S14). This enhancement is attributed to the increased availability of free surface sites for catalysis. Prior studies by Narayanan and El-Sayed have demonstrated that phenylboronic acid binds to these free sites through its hydroxyl group, effectively stabilizing the NP while positioning it for reaction with the aryl halide via collisional interactions.[20] By removing the capping agent, we increased the number of active sites, thereby enhancing the overall catalytic efficiency of the Pd NPs in the Suzuki coupling reaction.

Effect of Nanoparticle Size and Shape on Pd-Catalyzed Reactions. The catalytic activity of Pd NPs is influenced by several factors, particularly particle size and shape. Collins et al. have suggested that variations in catalytic performance among Pd NPs of different shapes may be attributed to different Pd leaching barriers.[8] Specifically, they observed that cubic Pd NPs exhibited more leaching given its higher surface energy to generate Pd(II) as the active catalyst, resulting in higher product yields compared to octahedral Pd NPs, with a reactivity trend of cubic NPs > cuboctahedral NPs > octahedral NPs.[9] To illustrate the utility of vT-DESI-MS in rapidly screening NP size and shape effects, we studied four Pd NP types (Table S4) using two reactions: (1) Suzuki coupling between phenylboronic acid and 2-bromo-5-methylpyridine (Figure 3) and (2) a tryptophan arylation (Figure S15). Results were analyzed in terms of both the effective surface area (Eff. SA) and the Pd concentration used in each reaction.

Effective Surface Area. The effective surface area refers to the portion of the NP surface that remains accessible for catalysis, which is reduced when the particles are immobilized on a solid substrate, compared to when they are dispersed in a bulk-phase reaction. As only the exposed facets are catalytically active, this factor plays a critical role in reactivity. By normalizing conversion ratios (based on MS intensities) to Eff. SA, we compared the intrinsic catalytic efficiency for both Suzuki coupling and tryptophan arylation at a fixed Pd concentration (1 ppm). For the Suzuki coupling reaction, the reactivity trend observed was 10 nm cubic NPs > 15 nm cubic NPs > 20 nm octahedral NPs > 20 nm cubic NPs (Figure 4a). Notably, the 10 nm cubic Pd NPs yielded a 10× higher conversion compared to the 20 nm cubic NPs. This finding indicates that as the effective surface area increases, conversion efficiency improves, likely due to an ability to more easily form Pd(II) species. Interestingly, they had a similar Eff. SA (Table

https://doi.org/10.1021/acs.analchem.5c02537
Anal. Chem. 2025, 97, 19544−19551

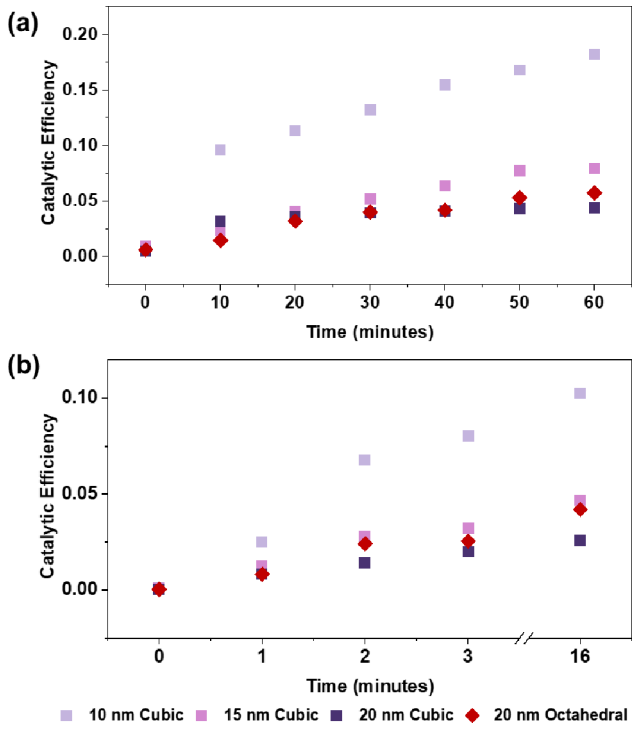

Figure 4. Conversion ratios normalized to the NP effective surface area for Pd NP-catalyzed (a) Suzuki coupling and (b) tryptophan arylation.

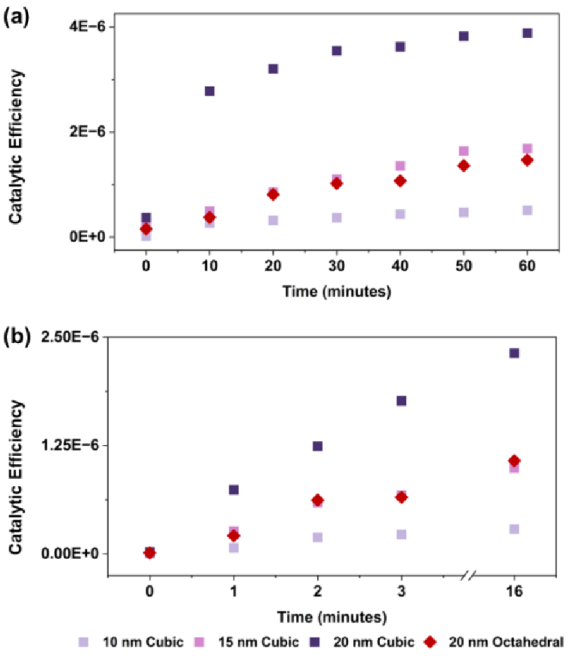

Figure 5. Conversion ratios normalized to the NP number for Pd NP-catalyzed (a) Suzuki coupling and (b) tryptophan arylation.

S4) to the 15 nm cubic Pd NP sample; the 20 nm octahedral Pd NP sample behaved more like the 20 nm cubic NP. This finding is attributed to the facet differences; cubic NPs expose {100} facets, which are higher in energy and provide more reactive sites compared to octahedral NPs, which predominantly expose {111} facets. Lower catalytic efficiency was observed in the Suzuki coupling reaction when octahedral nanoparticles (20 nm) were used compared to cubic nanoparticles (15 nm) with a similar effective surface area, highlighting the influence of nanoparticle shape on catalytic performance.

A similar trend was observed for the tryptophan arylation reaction (Figure 4b): 10 nm cubic NPs > 15 nm cubic NPs > 20 nm octahedral NPs > 20 nm cubic NPs. However, in this case, the 20 nm octahedral NP sample showed activity closer to that of the 15 nm cubic NP sample, suggesting a reduced impact of facet effects in this reaction system.

Pd Concentration. To assess how the NP number influences catalysis, we normalized the conversion ratio by the number of NPs used in each reaction (still at 1 ppm total Pd content). As larger NPs have more mass per particle, fewer are used per reaction compared with smaller ones. In both reactions, the reactivity trend normalized to the NP number was 20 nm cubic NPs > 15 nm cubic NPs ≈ 20 nm octahedral NPs > 10 nm cubic NPs (Figure 5a,b). This trend reverses the surface area normalization results and highlights the influence of particle count (i.e., the total available surface) on specific facet availability. Interestingly, the 20 nm octahedral and 15 nm cubic NPs had nearly identical reactivity, likely due to similar particle counts, suggesting that size and concentration effects outweigh facet-specific differences in this case.

Nanoparticle Discrimination. To further differentiate the NP catalytic behavior, we performed 240 Suzuki coupling reactions by varying the NP catalysts and reaction times. The conversion ratios shown in Figure 6 were calculated from MS ion intensities as the ratio of product ion to the sum of product

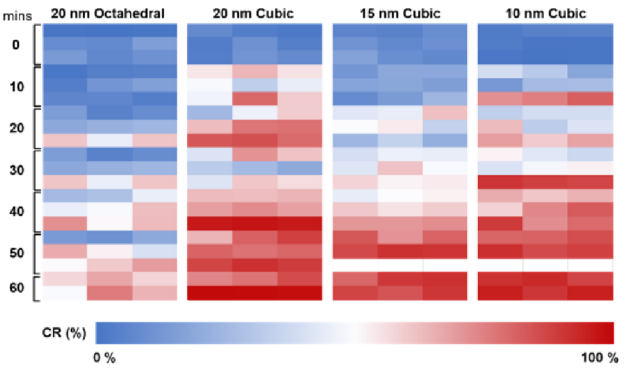

Figure 6. Heat map of Suzuki coupling conversion ratios across time for four Pd NPs (20 nm octahedral, 20 nm cubic, 15 nm cubic, and 10 nm cubic NPs) with darker blue representing 0% conversion and dark red indicating 100%. From top to bottom shows the reaction times (0, 10, 20, 30, 40, 50, and 60 min).

and reactant ions (eq S1). The heat map illustrates time-resolved catalytic performance, with darker blue representing 0% conversion and dark red indicating 100%.

To confirm the statistical significance of differences between NP shapes and sizes, we conducted principal component analysis (PCA) on the full MS data set (Figure 7). PCA results revealed clear discrimination between small (10 and 15 nm cubic Pd) NPs and large (20 nm cubic and 20 nm octahedral Pd) NPs (Figure 7a) possibly lending insights into size-dependent catalytic efficiency. Further separation was seen between the small NPs across different time points, with particularly distinct time-resolved clustering for the 10 nm cubic NPs (Figure 7b). Notably, PCA highlighted a distinct separation between early (≤20 min) and late (≥30 min) catalytic activity for the 10 nm cubic NPs. This differentiation could be due to the rise of different intermediates and final

https://doi.org/10.1021/acs.analchem.5c02537
Anal. Chem. 2025, 97, 19544−19551

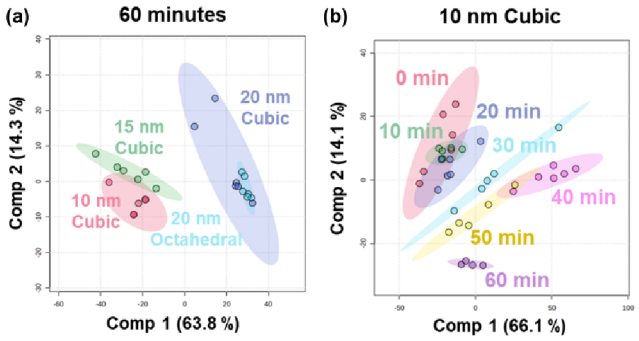

Figure 7. PCA plots showing NP discrimination based on catalytic activity: (a) all NPs (20 nm octahedral, 20 nm cubic, 15 nm cubic, and 10 nm cubic NPs for Suzuki coupling) at 60 min. (b) Time-resolved activity of 10 nm cubic NPs.

product conversion, which could be used to gain a better understanding of some reaction mechanisms.

CONCLUSIONS

In this study, we present a novel high-throughput catalysis platform that integrates thin-film reactions with variable-temperature desorption electrospray ionization mass spectrometry (HT-vT-DESI-MS), enabling a rapid and mechanistically insightful analysis of NP-catalyzed reactions. Utilizing this platform, we systematically investigated the effects of Pd NP size and morphology on the Suzuki cross-coupling reaction and tryptophan arylation. Our findings reveal that increasing the edge length of cubic Pd NPs from 10 to 20 nm significantly diminishes catalytic activity, a trend attributed to a reduced effective surface area and lower NP number density at constant Pd concentration. Furthermore, transitioning from cubic to octahedral NP geometry resulted in a marked decrease in product conversion, underscoring the influence of the surface facet structure on catalytic performance.

By coupling accelerated thin-film reactivity with precise temperature control and high-throughput MS detection, this platform enables reaction rates and analytical throughput far exceeding those of conventional bulk-phase methodologies. Under heated thin-film conditions, we observed up to a 10-fold increase in conversion rates compared with the same reaction completed in bulk solution, highlighting the synergistic benefits of simultaneous heating and real-time analysis. Additionally, the removal of capping agents further enhanced catalytic efficiency, likely by improving access to reactive surface sites.

Collectively, this work establishes HT-vT-DESI-MS as a powerful and versatile tool for uncovering nuanced structure–activity relationships and expediting the rational development of next-generation NP catalysts. The platform offers a robust, flexible, and efficient workflow for the rapid screening and optimization of heterogeneous catalytic systems with broad applicability across diverse reaction classes and catalyst architectures.

ASSOCIATED CONTENT

Supporting Information

The Supporting Information is available free of charge at https://pubs.acs.org/doi/10.1021/acs.analchem.5c02537.

Synthesis of palladium nanoparticles, spraying of NPs onto a DESI substrate, pneumatic sprayer parameters, platform using an external heating incubation chamber, variable-temperature DESI platform, accelerated Suzuki coupling conducted via microdroplet thin-film conditions, effect of capping agent removal on catalytic activity in the Suzuki coupling reaction, accelerated tryptophan arylation conducted via microdroplet thin-film conditions versus the bulk solution phase, and effect of NP size and shape on NP-catalyzed reactions (PDF)

AUTHOR INFORMATION

Corresponding Authors

Lane A. Baker − *Department of Chemistry, Texas A&M University, College Station, Texas 77843, United States;* orcid.org/0000-0001-5127-507X; Email: lane.baker@chem.tamu.edu

Sara E. Skrabalak − *Department of Chemistry, Indiana University-Bloomington, Bloomington, Indiana 47405, United States;* orcid.org/0000-0002-1873-100X; Email: sskrabal@iu.edu

Xin Yan − *Department of Chemistry, Texas A&M University, College Station, Texas 77843, United States;* orcid.org/0000-0002-8292-130X; Email: xyan@tamu.edu

Authors

Madison E. Edwards − *Department of Chemistry, Texas A&M University, College Station, Texas 77843, United States;* orcid.org/0000-0002-0041-5017

Nabojit Kar − *Department of Chemistry, Indiana University-Bloomington, Bloomington, Indiana 47405, United States;* orcid.org/0000-0003-0195-460X

Dallas P. Freitas − *Department of Chemistry, Texas A&M University, College Station, Texas 77843, United States;* orcid.org/0000-0003-2957-4158

Lingjie Zhang − *Department of Chemistry, Texas A&M University, College Station, Texas 77843, United States;* orcid.org/0000-0002-5183-465X

Oluwasegun J. Wahab − *Department of Chemistry, Texas A&M University, College Station, Texas 77843, United States;* orcid.org/0000-0003-4280-9089

Complete contact information is available at: https://pubs.acs.org/10.1021/acs.analchem.5c02537

Author Contributions

‡M.E.E., N.K., and D.P.F. contributed equally.

Notes

The authors declare no competing financial interest.

ACKNOWLEDGMENTS

This research was supported by the NSF Center for Chemical Innovation−The Center for Single-Entity Nanochemistry and Nanocrystal Design (Grant no. CHE-2221062). M.E.E. is thankful for the support from the NSF Graduate Research Fellowships Program (2139772). SEM imaging was conducted at the Texas A&M University Materials Characterization Core Facility (RRID SCR_022202). TEM imaging and XPS analysis were conducted at the Nanoscale Characterization Facility at Indiana University-Bloomington.

REFERENCES

(1) Reetz, M. T.; Breinbauer, R.; Wanninger, K. *Tetrahedron Lett.* **1996**, *37* (26), 4499−4502.

(2) Reetz, M. T.; Lohmer, G. *Chem. Commun.* **1996**, No. 16, 1921−1922.

(3) Kogan, V.; Aizenshtat, Z.; Popovitz-Biro, R.; Neumann, R. *Org. Lett.* **2002**, *4* (20), 3529−3532.

(4) Choudary, B. M.; Madhi, S.; Chowdari, N. S.; Kantam, M. L.; Sreedhar, B. *J. Am. Chem. Soc.* **2002**, *124* (47), 14127−14136.
(5) Reetz, M. T.; Westermann, E. *Angew. Chem., Int. Ed.* **2000**, *39* (1), 165−168.
(6) Son, S. U.; Park, K. H.; Chung, Y. K. *J. Am. Chem. Soc.* **2002**, *124* (24), 6838−6839.
(7) Park, K. H.; Son, S. U.; Chung, Y. K. *Org. Lett.* **2002**, *4* (24), 4361−4363.
(8) Collins, G.; Schmidt, M.; O'Dwyer, C.; McGlacken, G.; Holmes, J. D. *ACS Catal.* **2014**, *4* (9), 3105−3111.
(9) Nguyen, Q. N.; Wang, C.; Shang, Y.; Janssen, A.; Xia, Y. *Chem. Rev.* **2023**, *123* (7), 3693−3760.
(10) Tao, A. R.; Habas, S.; Yang, P. *small* **2008**, *4* (3), 310−325.
(11) Collins, G.; Schmidt, M.; O'Dwyer, C.; Holmes, J. D.; McGlacken, G. P. *Angew. Chem., Int. Ed.* **2014**, *53* (16), 4142−4145.
(12) Banerjee, S.; Basheer, C.; Zare, R. N. *Angew. Chem., Int. Ed.* **2016**, *55* (41), 12807−12811.
(13) Yan, X.; Augusti, R.; Li, X.; Cooks, R. G. *ChemPlusChem.* **2013**, *78* (9), 1142−1148.
(14) Wei, Z.; Li, Y.; Cooks, R. G.; Yan, X. *Annu. Rev. Phys. Chem.* **2020**, *71* (1), 31−51.
(15) Vernon, K. L.; Pungsrisai, T.; Wahab, O. J.; Alden, S. E.; Zhong, Y.; Choi, M. H.; Verma, E.; Bentley, A. K.; Bailey, K. O.; Skrabalak, S. E.; Ye, X.; Willets, K. A.; Baker, L. A. *ACS Electrochem.* **2024**, *1* (1), 93−102.
(16) Peng, H.-C.; Xie, S.; Park, J.; Xia, X.; Xia, Y. *J. Am. Chem. Soc.* **2013**, *135* (10), 3780−3783.
(17) Jin, M.; Zhang, H.; Xie, Z.; Xia, Y. *Angew. Chem., Int. Ed.* **2011**, *50* (34), 7850−7854.
(18) Tucker, L. H.; Conde-González, A.; Cobice, D.; Hamm, G. R.; Goodwin, R. J.; Campbell, C. J.; Clarke, D. J.; Mackay, C. L. *Anal. Chem.* **2018**, *90* (15), 8742−8749.
(19) Brown, H. M.; Fedick, P. W. *Reaction Chemistry & Engineering* **2023**, *8* (3), 556−562.
(20) Narayanan, R.; El-Sayed, M. A. *J. Am. Chem. Soc.* **2003**, *125* (27), 8340−8347.

https://doi.org/10.1021/acs.analchem.5c02537
Anal. Chem. 2025, 97, 19544−19551